OPTIMIZATION OF THE HETS HE-COOLED DIVERTOR CONCEPT: THERMAL FLUID AND STRUCTURAL ANALYSIS

Panos J. Karditsas

EURATOM/UKAEA Fusion Association, Culham Science Centre, Abingdon, Oxfordshire OX14 3DB, UK
panos.karditsas@ukaea.org.uk

The High Efficiency Thermal Shield (HETS) concept was proposed by ENEA for divertor application in the context of the ITER project and as part of the European Power Plant Conceptual Study. The design is modular, and the unit dimensions are of the order of centimeters for limiting mechanical and thermal stresses. This paper presents results of thermal-fluid and structural analyses, with different heat flux loads, fluid pressures and inlet velocities. The fluid analysis shows that the sharp corner flow passage at the point of flow reversal behaves like an abrupt enlargement, leading to considerable pressure losses as compared to the results obtained by rounding the corner. The combination of rounding the sharp corner and flow cross-sectional area expansion, leads to reduced pressure losses, without any degradation of the thermal performance of the component.

I. INTRODUCTION

Divertor design concepts were studied as part of the European Power Plant Conceptual Study. Primary requirements were operation with high temperature helium for better thermodynamic efficiency, and the ability to withstand 10 MW/m^2 of incident flux.

The requirement for high temperature operation led the structural material choices to be tungsten for the armour, and tungsten alloy for the pressure-retaining boundary. Tungsten and alloys have an operating temperature range 300-1300^{o}C, limited by the ductile to brittle transition (DBT) and recrystallisation temperatures respectively. The DBT temperature under fusion neutron irradiation is estimated to be around 600^{o}C, which narrows the "design window" to a range of 600-1300^{o}C. The coolant is helium gas operated at pressures in the range 10-14 MPa with inlet temperatures in the range of 600-800^{o}C. The final choice of operating parameters involves the choice of mass flow rate, to keep temperature values within the structural material operating limits, and pressure drop and pumping power to a minimum. Details of the design can be found in[1,2]. The schematic cut-away of the section used in this study for the finite element calculations is shown in Fig. 1. The basic feature of the design is flow of coolant at high speed through a narrow channel of width in the range 0.9-2mm, and the use of tungsten alloy as the pressure retaining material. Finite element calculations were performed with various heat flux loads, fluid pressures and flow speeds (i.e. mass flow rates), using the commercially available fluid dynamics code FlowPlus[3], the fluid module of the COSMOS/M[4] family of solvers. Linear elastic structural analysis was also performed, to deduce the pressure and thermally induced stresses and strains. A shape optimised for flow is proposed, and a schematic is shown in Fig. 2.

II. GENERAL DESIGN FEATURES

The HETS design adopted (Fig. 1) is axisymmetric in the vertical direction, smeared from the 35 mm hexagonal original shape The design was first developed for low temperature operation (~50^{o}C) with pressurised water as the coolant, and tests[5] were carried out demonstrating capability to withstand ~40 MW/m^2. In a previous study[6], two cases were investigated with helium inlet temperatures of 600^{o}C and 800^{o}C, flow velocity 230 m/s, and pressure 14 MPa, with mass flow of 0.0675 kg/s and 0.055 kg/s respectively, resulting in static pressure losses of 0.18 MPa, and thermal behaviour within limits. These results led to the more precise definition of the operating range and target values of parameters used in this study. The required mass flow rate is 0.0713 kg/s, with an inlet temperature of 600^{o}C to satisfy the lower limit of temperature (due to DBT). Two coolant pressure values were used for analysis: 14 MPa and 10 MPa, to examine the effect on flow, and achieve lower primary stresses. Flow goes through P6=3.5 mm radius nozzle, impinges on the heated part of the structure, side P5=18.5 mm, and then is diverted sideways through the narrow channel of P1=1.8 mm height at inlet and P2=0.9 mm at exit. All highlighted sections (P1-P6) have the same dimensions, with P3=1.5 mm, and P4=5.0 mm. The dome and fillet in II have radii of 10 mm and 0.5 mm. The compliant soft (braze) layer, i.e. the thin layer of material between the top surface of the dome and the lower surface of the armour, is 0.1mm thick in both I and II.

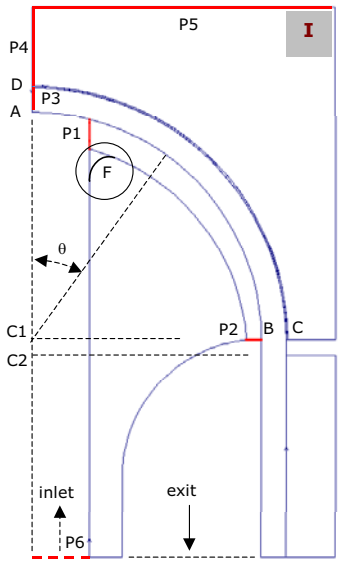

Fig 1: Schematic of the computational section used for the reference HETS divertor design (I).

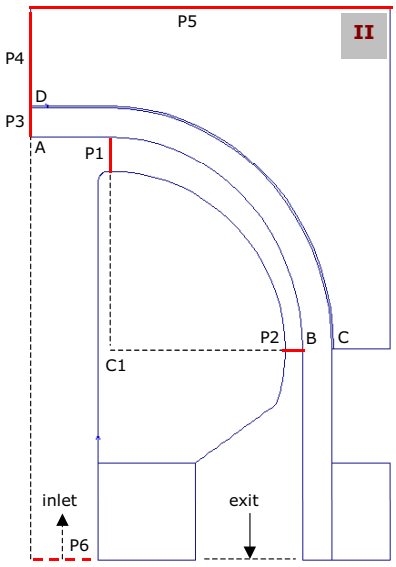

Fig 2: Schematic of the computational section used for the proposed "optimised for flow" shape (II).

II.A. Performance issues and parameters

Fluid flow through narrow passages results in compression and expansion with frictional losses at the boundaries. In general the total P (MPa), can be expressed in terms of the static pressure p (MPa), and a dynamic term:

$$P = p + \frac{\rho V^2}{2} = p + \frac{1}{2}\left(\frac{\dot{m}}{A_x}\right)^2 \rho^{-1} \qquad (1)$$

with $\dot{m}$ (kg/s) the mass flow rate, V (m/s) the flow velocity, ρ (kg/m^3) the density, and A_x (m^2) the flow cross sectional area. The pressure losses between inlet (suffix 1) and exit (suffix 2) result in pumping power demand of $\dot{W}_{pump}$ (W).

For a given mass flow rate, pumping power is proportional to (density)$^{-2}$, as the pressure drop ΔP is proportional to (density)$^{-1}$.

The static pressure p and its change throughout the flow field depend on the local flow velocity and on the shape (cross sectional area, perimeter and length) of the passage (channel). Whether the component behaves as an abrupt enlargement/contraction, or a diffuser/nozzle depends on the "sharpness" of these features and the way the cross sectional area changes in the flow direction. Abrupt enlargement or contraction behaviour leads to significant pressure losses, but a diffuser behaviour can lead to increases of static pressure.

In the component under investigation, where the geometry changes radically in the flow direction, the change of static pressure depends heavily on features of the channel, such as the sharp corner of Fig. 1. The cross sectional area increases from 4.024E-4 m^2 (section P1) to 7.644E-4 m^2 (section P2), an expansion ratio 1.9, with the potential of the channel to act either as a diffuser or as an abrupt enlargement.

III. RESULTS AND DISCUSSION

Using commercially available finite element computer codes, fluid calculations were performed on sections of the proposed divertor designs using FlowPlus[3], and structural analysis using COSMOS/M[4].

III.A. Thermal fluid analysis

Referring to Fig. 1, contour (AB) marks the path for the wall and fluid temperatures, and the effective values of the heat transfer coefficient. Contour (CD) marks the interface (soft layer/braze) between the W-alloy structural dome and the W-armour.

The effective heat transfer coefficient is based on the local heat transfer between solid and fluid, and the fluid and wall temperatures, as calculated by the finite element analysis, and is not a predetermined input parameter.

The inlet temperature of 600°C was not varied, because previous calculations with higher inlet temperatures resulted in structural temperatures above the 1300°C limit set here for reliable operation of the component. The target mass flow rate for the reference design was set at 0.07 kg/s. Table I summarises the cases studied and lists the principal input parameters for every case investigated.

TABLE I. Principal input parameters

case	Q (MW/m^2)	P (bar)	$\dot{m}$ (kg/s)	V_1 (m/s)	T_1 (°C)
2	10	140	0.0520	175	600
3	10	140	0.0594	200	600
1 ref	**10**	**140**	**0.0713**	**240**	**600**
4	10	140	0.0817	275	600
5	10	140	0.0891	300	600
1b	15	140	0.0713	240	600
1c	20	140	0.0713	240	600
1 opt	**10**	**140**	**0.0713**	**240**	**600**
1d	10	100	0.0700	330	600

Some of the principal output parameters, i.e. maximum W-alloy dome (fluid and armour side), and maximum W-armour temperatures, total pressure loss ΔP, and required pump power per unit $\dot{W}_{pump}$, are given in Table II.

TABLE II. Principal ouput parameters

	$T_{(max)}$ dome side (°C)		$T_{(max)}$ armour (°C)	ΔP (kPa)	W_{pump} /unit (kW)
	fluid	armour			
2	1146.3	1344.4	2186.7	207.3	1.396
3	1083.0	1281.8	2128.3	269.8	2.077
1 ref	**1009.6**	**1209.4**	**2059.0**	**387.0**	**3.575**
4	961.0	1162.2	2013.7	508.0	5.376
5	933.5	1135.4	1987.4	632.6	7.303
1b	1256.9	1568.4	2899.9	388.7	3.590
1c	1527.6	1959.9	3754.8	390.4	3.606
1 opt	**1097.8**	**1273.4**	**2034.5**	**99.1**	**0.916**
1d	1039.4	1242.1	2106.2	518.6	6.586

*W-armour melting point temperature is 3410°C.

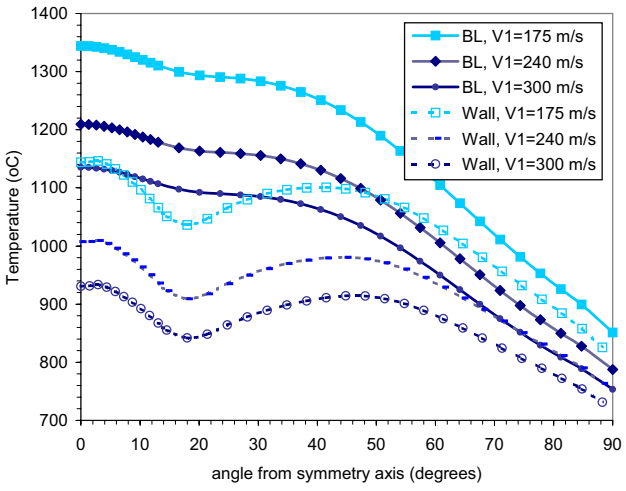

Fig 3: The variation of wall (AB) and braze layer (CD) temperature with angle from the symmetry axis.

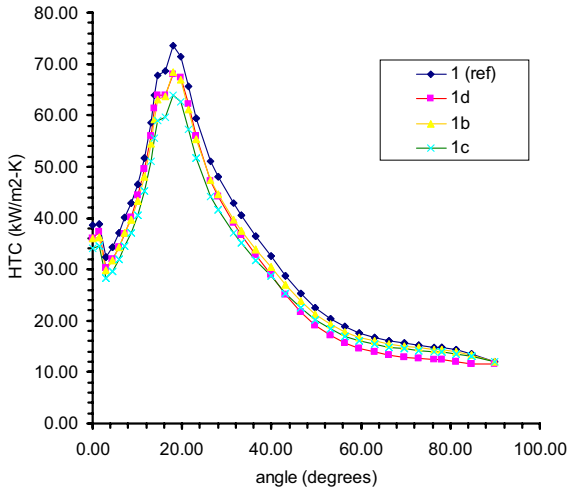

Fig 4: Variation of effective heat transfer coefficient with angle from symmetry axis.

Figure 3 shows the variation of wall (contour AB) and braze layer (contour CD) temperature with angle from the symmetry axis, with the effect of coolant velocity (i.e. mass flow rate). Figure 4 shows the variation of effective heat transfer coefficient for surface (AB), as normalised to a uniform coolant temperature of 600°C, with angle from the symmetry axis, for cases 1(ref), 1d, 1b, and 1c. Figures 5-6 show the distribution of velocity magnitude in the component for the 1(ref) and 1(opt) cases, with surface heat flux value 10 MW/m^2. Figure 7 shows the stress intensity in the component for the reference case.

The static pressure loss depends on frictional and form drag. Flows with constant cross sectional area lead to losses from frictional drag, but variations of flow channel geometry, lead to additional "form" effects. The increased losses of case 1(ref) are entirely due to the sharp corner around point F (Fig. 1). A comparison of the flow fields between the sharp and rounded cases (Figs. 5, 6) shows a much larger re-circulation region R in the sharp corner area. Rounding leads to smooth transition and a "gentle" flow pattern in the 90+ degree bend of the flow.

Case 1(opt) attempts to increase the flow around the stagnation point in order to lower temperatures, and eases the transition on exiting the narrow section P2.

The temperature difference across the section of the dome (fluid to armour side) induces thermal stresses. It is typically ~200 K in the hotter regions and ~30 K towards the flow exit region, with the exception just beyond the sharp corner, where it is ~280 K. This enhanced "cooling" effect is due to the flow pattern: as the flow speeds up and clears the sharp bend, it appears "splashing" towards the top surface of the channel (Figs. 5-6). This increase in temperature gradient results in an increase of the thermal stress in that region. The a posteriori calculated heat transfer coefficient values show a strong dependence on

flow velocity and a smaller dependence on surface heat flux or coolant pressure variations. They show a peak in the region just beyond the sharp corner, with values in the range of 50-90 kW/m^2-K. Reducing the operating pressure from 14 MPa to 10 MPa does not have a pronounced effect on the thermal performance of the component or the flow velocity distribution (although the actual flow velocity is higher), but it does result in higher-pressure losses due to the lower coolant density. The coolant temperature rise is ~40 K.

III.B. Structural analysis

Linear elastic calculations on the reference HETS concept involved stresses and strains induced by the internal pressure of the coolant (p=10 MPa, 14 MPa), and temperature gradients due to the applied heat flux, allowing for a "soft" layer between the tungsten alloy dome and the tungsten armour. It is assumed that this layer's function is to minimise stress transmission between the armour and the structural dome.

Calculations performed on the hemispherical dome determine the primary membrane P_m (MPa), local membrane P_L, bending P_b and secondary thermal Q_R stresses, across a typical section. Section CC is the location of the calculated maximum stresses and strains. When the stress distribution is integrated over section CC (Fig. 7), the primary membrane and bending components (linearised across the section) of the stress are obtained. The relevant values of stresses, strains and limits, are given in Table IV.

TABLE IV. Stress-strain and limits

Parameter	P=10 MPa		P=14 MPa	
Maximum strain %	0.123		0.123	
Average strain %	0.0553		0.0543	
P_m (MPa)	44.8		62.7	
Average temp (^{o}C)	1078.6		1091.5	
P_b (MPa)	12.0		16.7	
All in MPa	Max. S	Max. T	Max. S	Max. T
S	540.9	144.0	542.2	121.0
Q_R	486.9	184.6	466.7	177.9
P_L	54.0	40.6	75.5	56.9
$P_L + P_b/K_t$	63.6	50.2	88.9	70.3
$(P_L + P_b)/K$	44.0	35.0	61.5	49.0
$\boldsymbol{S_y}$	**383.0**	**284.0**	**373.5**	**285.4**
$\boldsymbol{S_m}$	**119.0**	**92.6**	**115.8**	**92.9**
$X = (P_L + P_b/K_t)/S_y$	0.166	0.177	0.238	0.246
$Y = Q_R/S_y$	1.271	0.650	1.250	0.623
$X + Y/4$	0.484	0.340	0.550	0.401

*The value of Kt=1.25 and of K=1.5. Bold characters designate material properties and not calculated parameters. Max. S:values at location of maximum stress. Max. T:values at location of maximum temperature.

The structural analysis results demonstrate that static stress requirements, including limits for stress concentration regions, are met or are within the uncertainties of the material properties used. The deformation limits are satisfied, as the strains calculated are within the 1% average and 5% local values specified in the design code, although an inelastic analysis might have produced higher values than the 0.123% calculated.

As the value of Y is greater than 1.0 (secondary stress above yield stress), part of section CC is within the plastic regime, but the structure is expected to shakedown back to elastic behaviour after a few applications of the load. The time dependent loads, including irradiation effects, and stress requirements are not accounted for in the above evaluation. Also, the stress for a continuous structure is above 1000 MPa.

IV. CONCLUSIONS

The results of calculations show that the maximum temperature for the reference case is within the operating limits of the structural material. The fluid dynamic calculations show that with very minor changes of the geometry (provided that the manufacturing will not be prohibitive), improvements on the pressure drop and the structural dome operating temperatures are possible. Results show that pressure, and its change throughout the flow field, depends on local flow velocity and channel shape. Most of the cases studied exhibited significant pressure losses, but the "optimised for flow" case led to smaller total pressure loss.

The elastic thermal-structural analysis shows that, excluding neutron irradiation effects, the material could withstand the stresses from internal pressure and temperature gradients, thus satisfying static stress and strain requirements. The time dependent loads, stress requirements, and the effects of exposure to loads for a large duration of time at high temperature in a fusion power plant, need to be further assessed. Relevant tungsten and alloy data for thermal creep, and neutron irradiation effects are required. Critical issues are:

(a) irradiation creep and its effect on the stress-to-rupture values for the material,

(b) embrittlement and its effects on ductility, and the deformation limits,

(c) degradation of thermal conductivity[7], as much as 24% at a dose of 4 dpa, which results in higher temperatures in the solid, thus lowering the static stress limits.

Further studies are needed, varying the geometry and the operating conditions. Also, experiments to confirm performance are required.

ACKNOWLEDGMENTS

The author would like to thank Mr Raoul Pampin for running the FlowPlus finite element code on his behalf. This work was funded jointly by the United Kingdom Engineering and Physical Sciences Research Council and by EURATOM.

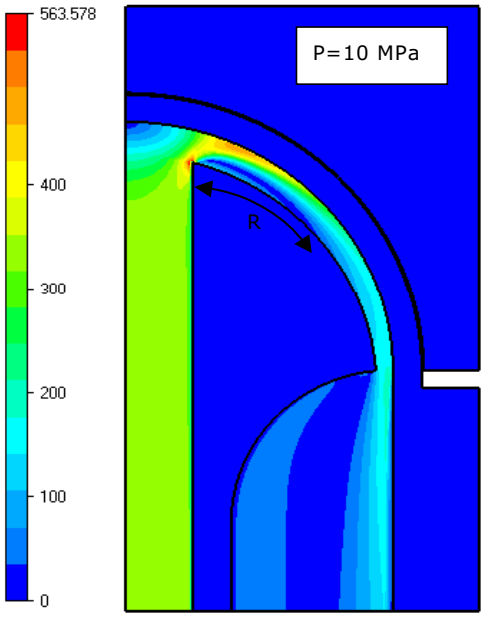

Fig 5: The velocity distribution for case 1(ref), Q=10MW/m^2.

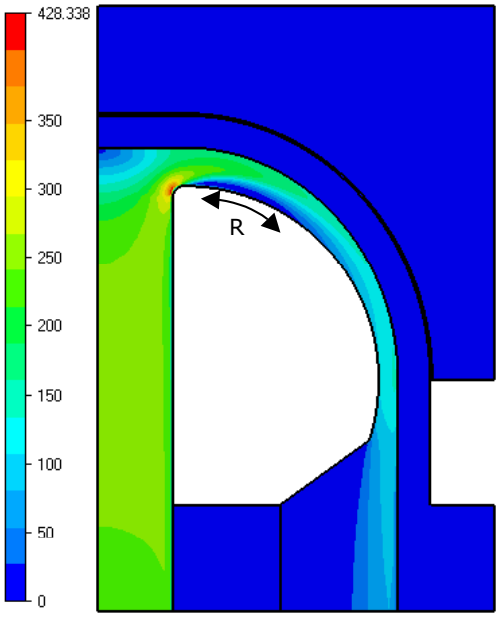

Fig 6: The velocity distribution for case 1(opt) with pressure p=14 MPa and Q=10 MW/m^2.

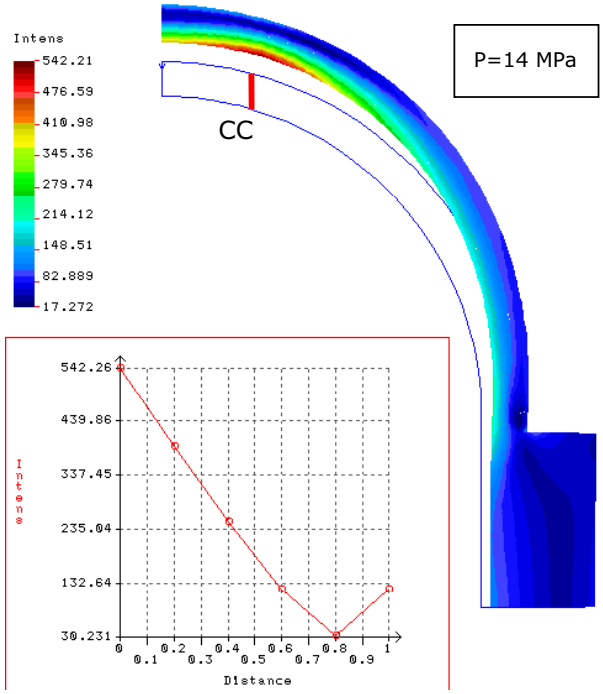

Fig 7: The stress intensity distribution in the structural dome and support due to the combined loads of coolant internal pressure and surface heat flux, and the variation across section CC, case 1(ref).

REFERENCES

[1] S. Hermsmeyer, S. Malang, 'Gas-cooled high performance divertor for a power plant', Proc. ISFNT-6, San Diego, USA (2002).

[2] A. Pizzuto et. al., 'Draft of Interim report for Task-PPCS-10: Alternative helium cooled divertor concept', ENEA, Frascati, Italy (2002).

[3] Blue Ridge Numerics Inc., "FlowPlus v5.0: Finite element fluid flow and heat transfer solver", Charlottesville, VA, USA (2002).

[4] Structural Research and Analysis Corp., COSMOS/M v2.7: A complete finite element analysis system, Santa Monica, CA, USA (2002).

[5] A. Pizzuto, B. Riccardi, "Preliminary critical heat flux assessment of the High Efficiency Thermal Shield device", Transactions of XVI IEEE/MPTS SOFE (1995).

[6] P.J. Karditsas and N.P. Taylor, "Thermal fluid finite element calculations for the European PPCS divertor concepts", Fusion science and Technology 44, No.1 (2003).

[7] ITER MPH-IV, "Materials Properties Handbook for vessel and in-vessel components", G74 MA 9 01-07-11 W 0.2 (2000).